Scientific Reports

https://doi.org/10.1038/s41598-026-66753-1

Article in Press

Spiders' gyroscopic motion via web mechanical intelligence facilitates prey sensing

Received: 5 June 2026

Accepted: 10 August 2026

Published online: 19 August 2026

Cite this article as: Masmeijer T.C.P., Slavič J., De P. *et al.* Spiders' gyroscopic motion via web mechanical intelligence facilitates prey sensing. *Sci Rep* (2026). https://doi.org/10.1038/s41598-026-66753-1

T. C. P. Masmeijer, J. Slavič, P. De, T. A. Blackledge & E. Habtour

Spiders' Gyroscopic Motion via Web Mechanical Intelligence Facilitates Prey Sensing

T.C.P. Masmeijer[1], J. Slavič[2], P. De [3], T.A. Blackledge[3], E. Habtour[4*]

[1]Applied Mechanics & Data Analysis, University of Twente, Enschede, Netherlands.

[2]Faculty of Mechanical Engineering, University of Ljubljana, Ljubljana, Slovenia.

[3]Department of Biology and Integrated Bioscience Program, University of Akron, USA.

[4]Aeronautics & Astronautics Department, University of Washington, Seattle, USA.

*Corresponding author. Email: habtour@uw.edu

Significance

This work reshapes our understanding of how miniature animals perform rapid, complex sensing by revealing that spiders outsource some cognitive tasks to their webs rather than their nervous systems. Despite their poor vision, tiny brains, and imprecise web geometries, spiders must instantly sense the mass and location of prey on their webs. This capability is achieved through the mechanical inelegance of web design, which makes it insensitive to the inherent imprecision and irregularities in web construction. The findings suggest that, in addition to using their legs as a sensory array, spiders use the pitch and roll of their bodies on floppy webs to rapidly localize prey. In addition to revealing a new sensory mechanism for spiders, this study offers a blueprint for engineered structures that perform sensing and decision-making through structural geometries and dynamics rather than electronics.

Abstract

Orb-weaving spiders must localize and size prey rapidly upon impact, despite their poor vision and small brains. Leading hypotheses suggest that the local material intelligence of orb web threads enables spiders to tune them individually to resolve prey location and mass cues by decoding vibrations across the spider's eight independent legs—a task requiring high cognitive overhead if material intelligence is used alone due to the web's inherent geometric and material irregularities. Here, we reveal that an orb web also exhibits a form of global mechanical intelligence: the spider's entire body acts synergistically with the flexible web's global vibration motion as a gyroscope and cue decoder. Through extensive simulations and experiments, we demonstrate that impact events trigger specific pitch-roll dynamics in the spider's body, facilitated by the web architecture. These dynamics provide robust prey localization cues, without requiring processing of sensory input from eight individual legs; offloading some cognitive tasks onto the web. The findings reveal a novel source of information for spiders, and offer a blueprint for realizing transformative structures with cognitive functions.

1 Introduction

Orb-weaving spiders must rely on their webs not only to intercept prey but also to sense and interpret vibration signals generated by a prey's impact, struggle to free itself, or both (*1–4*). Because of their poor visual (*5, 6*) and limited neural processing capabilities (*7–9*), spiders leverage vibration signals to localize and distinguish prey from debris with remarkable speed, ≈10-100ms. Their rapid sensing is difficult to reconcile only under current hypotheses that each leg independently samples signals transmitted along individual silk threads (*10, 11*) and then reconstructs directional and mass cues about the prey (*12–14*). Those hypotheses assume spiders have detailed knowledge of the web's geometric and material properties (*15, 16*), and can interpret multiple asynchronous thread-scale signals. However, those assumptions require invariant web properties and substantial cognitive demands— memory allocation, signal filtering, and cue classification (*17, 18*). Neither requirement is plausible, given the inherently variable nature of web properties and the small brain size of spiders. Our findings demystify this contradiction by revealing that orb-webs may exhibit mechanical intelligence, as an extension of Marom-Buehler material intelligence in biological

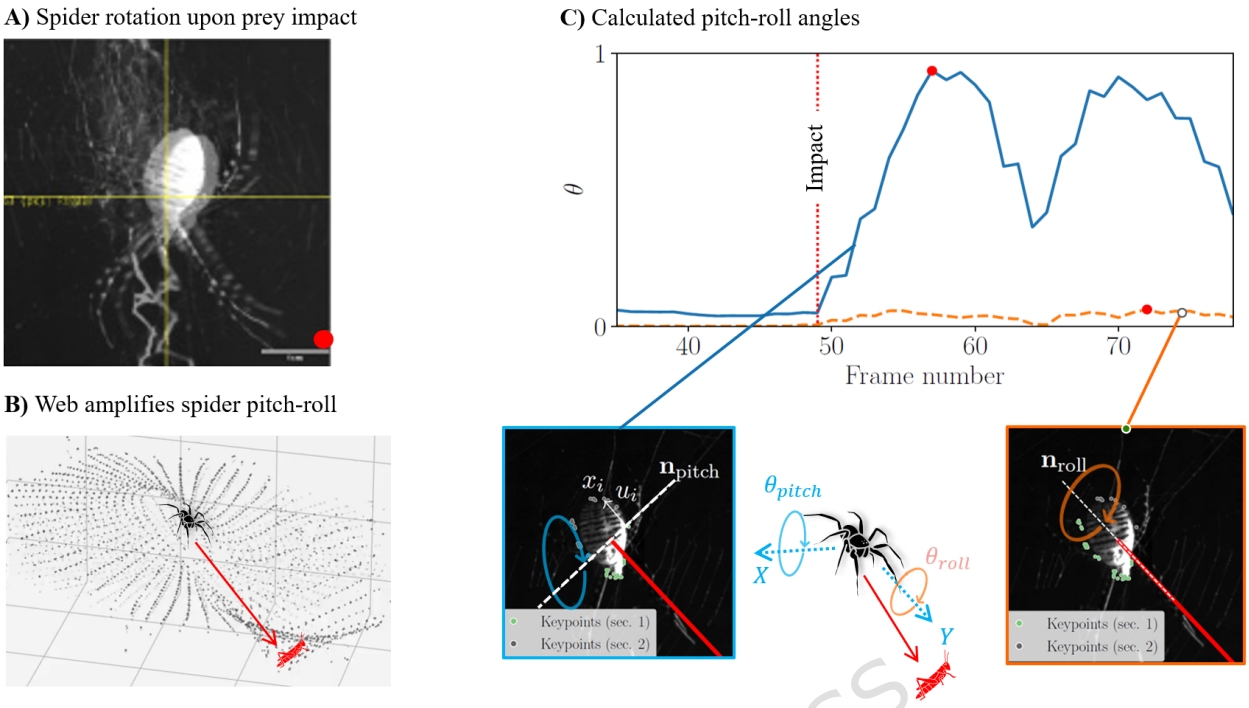

Figure 1: **Spider uses its entire body pitch-roll motion for sensing direction and mass of prey.** (**A**) An example of a spider's position before an impact is the solid image and its position during the maximum observed rotation is the translucent overlay. (**B**) The spider leverages its flexible web to transform impact-induced vibrations into a simple abdomen pitch-roll motion, allowing it to rapidly infer prey direction and size despite substantial natural variation in web geometric patterns. (**C**) The spider ignores the small roll angle, θ_{roll}, by making only a small trajectory adjustment toward the direction with the large pitch angle, θ_{pitch}, which is the prey direction. The full video is in movie S1, and the detailed analysis of the roll-pitch sequence is in figure S1.

structures (*19*). The web material and mechanical intelligence are controlled by the web's local material and global geometric properties. Both material and mechanical intelligence allow spiders to outsource energy-intensive cognitive tasks to their webs, including filtering vibration signals, cueing, and decoding. This study was focused on the web's mechanical intelligence, which causes spiders to pitch toward initial high impulses of prey impacts. We focus on impact events because they are the first possible sources of prey information for the spider.

Based on Marom-Buehler biological material intelligence framing, sensing capacity at the thread level can be attributed to material's capacity to passively process vibration waves (signals) through

adaptive structurally encoded microscopic or molecular logic rather than neural or electronic computation (*20*). From a classical mechanics perspective, thread material intelligence for sensing through spider legs is limited to low-amplitude and high-frequency vibrations, e.g, prey struggling to free itself from the sticky web or a spider feeling reflective waves after plucking the hub of its web. Hence, the focus of most previous investigations were on the spider legs' sensitivity to the thread signals at the web hub based on only low amplitude (≈ 0.2-2mm) and high frequency (200-1000 Hz) vibration waves, including square (*3, 21*), single harmonics (*22*), and broadband (*13*) signals. These excitation types were reasonable for simulating a struggling prey but not an impact event. Our study addressed this gap by demonstrating that the orb-web's global geometry exhibits mechanical intelligence for decoding high-amplitude impact signals. The findings show that an orb-web generates specific vibration shapes, called eigenmodes, as an embedded processor that maps prey impact onto the spider's entire-body pitch-roll (gyroscopic) cue, extending the spider-silk hierarchy from mechanical toughness into structurally embodied cognition.

The hypothesis of this study is that an orb spider may obtain prey direction and mass cues from an impact event, regardless of web shape or prey location. This was achieved by the spider simply using its body as a single pitch-roll locomotion sensor. Specifically, the web-spider symbiotic locomotion is analogous to a dual mechanical gyroscope and mass sensor. The orb web's structural flexibility and global landscape-scale design produce dominant deflection mode shapes that are contained in the vibration signals. Each mode has a specific shape, ϕ_n, that oscillates at high amplitude and low resonance frequency, ω_n. These modes produce unique distortions governed by the prey's specific size and impact location. Figure 1 illustrates how the flexible web of argiope trifasciata spider is distorted due to a cricket impact (Figure 1A) causes the entire spider's abdomen to experience a rocking motion (Figure 1B), manifested as pitch, θ_{pitch}, and roll θ_{roll} rotations (Figure 1C). The argiope trifasciata body feels a stronger pitch motion than roll, $\theta_{\text{pitch}} > \theta_{\text{roll}}$, which directs it toward the prey (Figure 1C). This suggests that orb-webs are a form of mechanical intelligence that focuses spiders on simple, easily interrupted low-frequency vibration signals; eliminating the need for sophisticated cognition to process complex, noisy high-frequency signals. The full video of the spider's use of the pitch-roll mechanism to capture its prey is provided in movie S1 with a breakdown of the mechanism in figure S1. The robustness of the pitch-roll sensing mechanism was observed in 10 videos of prey striking natural orb webs with spiders, and verified using 18,900

computational simulations and 74 experiments using artificial webs, as detailed in (*23*). Example files of movies, data, and simulation files are available in (*24*).

2 A spider body pitch-roll motion as a sensor for directional and mass cues

Cues from non-impact signals instigated by spiders plucking their web (*25*), or prey struggling to free themselves (*3*), are not considered here. Instead, we focused on prey impact since it precedes those events and is crucial for localization. Therefore, we isolated the physics governing this rapid directional and mass sensing upon impact, arising from the pitch-roll interplay between the spider and its web. Because orb webs are flexible, tensioned networks, their signal properties, namely resonance frequencies and deflection mode shapes, depend on the web's distributed tension, mass m_{web}, and global geometry. Across all web shapes, adding even a small prey mass, m_{prey}, substantially lowers ω_n and distorts ϕ_n, to produce a unique pitch-roll motion that informs prey direction; details provided in (*23*). To confirm the sensing robustness across the irregular shapes typical of natural orb-webs, which are often asymmetric and vertically elongated with the hub located above the geometric center (*26, 27*). To this end, three web shapes were investigated: nearly symmetric (Web 1: Ecc =0.03, Nar =0.07); moderately eccentric and narrow (Web 2: Ecc =-0.18, Nar =0.48); and highly eccentric and narrow (Web 3: Ecc =-0.26, Nar =0.64). The eccentricity and narrowness are given by: Ecc $= (L_{\text{upper}} - L_{\text{lower}})/(L_{\text{upper}} + L_{\text{lower}})$ and $\text{Nar}^2 = 1 - (L_{\text{hor}}/L_{\text{vert}})^2$, respectively (Figure 2A). Typical Ecc = values vary by species, e.g. *Araneus diadematus* and *Nephila clavipes* Ecc = −0.21 and −0.48, respectively (*26, 27*).

Despite the landscape-scale variation in vibration properties, all webs produced clear hub pitch–roll motion that reliably indicated prey impact direction without requiring signals through individual threads. Figure 2B illustrates clearly this effect for Web 2, where adding a prey mass as small as ∼10% of a fruit fly (equivalent to $m_{prey} \approx 0.1\%$ of $m_{spider+web}$ or equivalent to a dust particle), leads to significant reshaping of modes $n = \{2, 3, 5\}$; all of which involve twisting and containing nodes. In contrast, the first mode— a bell-like shape symmetric and node-free mode ——remains unchanged. The shapes remain unchanged for higher modes if the impact occurs at

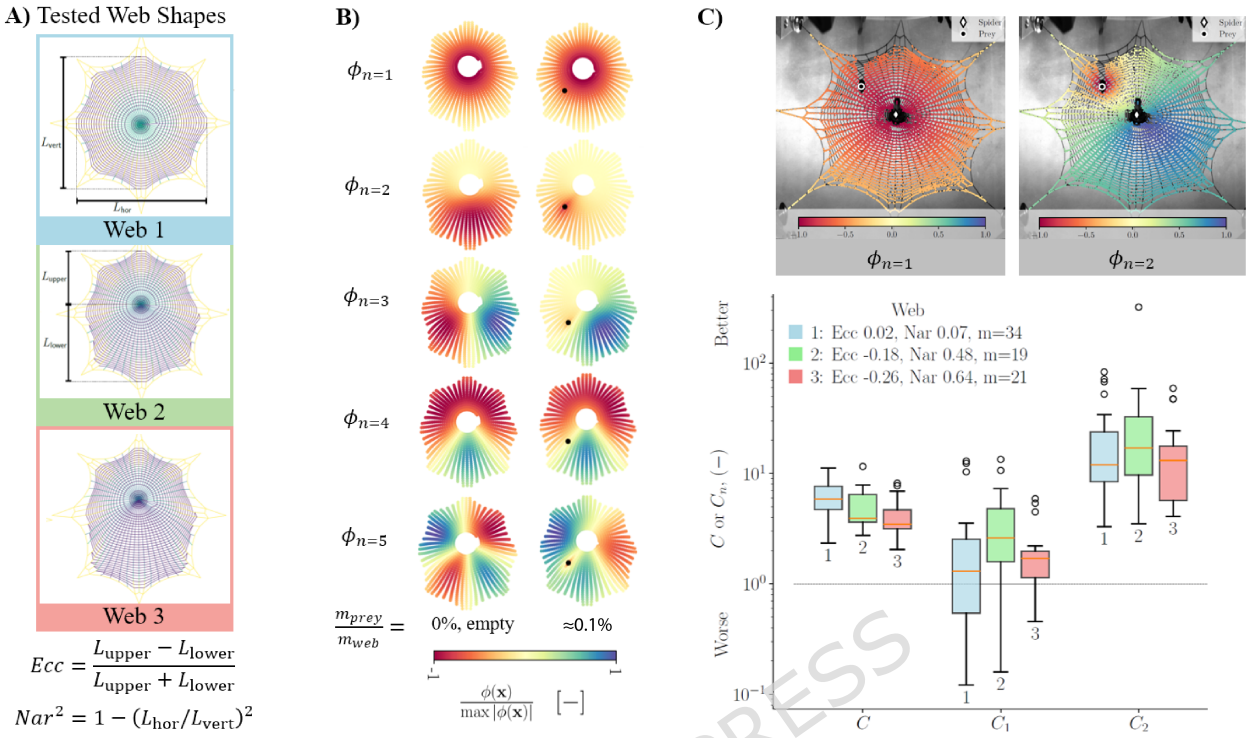

Figure 2: **A Spider pitch-roll sensing mechanism provides simple directional cue clarity regardless of web shapes.** (**A**) The pitch-roll robustness for sensing prey impact direction is verified for webs that are nearly symmetric (Web 1: Ecc=0.03, Nar=0.07), moderately eccentric and narrow (Web 2: Ecc=-0.18, Nar=0.48), and highly eccentric and narrow (Web 3: Ecc=-0.26, Nar=0.64). (**B**) Web 2 dynamic characterization simulations via finite element method (FEM) simulations show (in right column) drastic distortion in deflection mode-shapes $\phi_{n=2}$, $\phi_{n=3}$, and $\phi_{n=5}$ even for small impact of $m_{prey} \sim 0.001 m_{spider+web}$, or 10% of fruit fly mass, when compared to an empty web (left column). Similar findings for Web 1, 2, and 3 with different impact masses are shown in figures S3 to S8. (**C**) High-speed optical characterization of 3D-printed Web 2 dynamics agrees with FEM simulations. Note the similarity between the shapes of $\phi_{n=2}$ in (B) and (C) after impact, as detailed in (*23*). Experimental distributions of directional clarity metrics for three TPU web geometries. Boxplots show the variability across repeated impact experiments at different impact locations for the overall directional clarity C and the contributions from the first two modes, C_1 and C_2. Across all webs, C_2 consistently exceeded C_1, demonstrating the strong directional clarity associated with the second mode $\phi_{n=2}$.

a node. Hence no change in $\phi_{n=4}$ (Figure 2B). The simulations consisted of five prey masses, $m_{\text{prey}} = \{0.2, 2, 6, 20, 200\}$ mg. For brevity, the discussions are focused on $m_{\text{prey}} = \{0.2, 2, 20, 200\}$ mg corresponding to 10% fruit fly, full fruit fly, housefly, and cricket, respectively. While the pitch–roll mechanism provided both directional and mass cues, the directional cue was substantially clearer. Maps of the web dynamics as a function of prey masses are provided in figures S3 to S8.

3 Landscape-scale modes provide robust directional clarity across variable web geometries

Using only global landscape-scale signals as inputs (*13, 28*), we obtained the spider's whole-body rotations both computationally and experimentally, which provided physical insights into why the spider's pitch-roll motion is a plausible sensing mechanism. The strengths of the collective and modal (mode-shape) directional clarity are given, respectively, as:

$$\mathrm{C} = \frac{\max|\theta_{\text{pitch}}|}{\max|\theta_{\text{roll}}|} \qquad (1) \qquad\qquad \mathrm{C}_n = \frac{|\theta_{\text{pitch},n}|}{|\theta_{\text{roll},n}|} \qquad (2)$$

A high clarity of the prey impact directional cue requires $C > 1$. For example, the argiope trifasciata spider web yielded a high directional cue of $C = 14.8$, which meant the pitch motion was nearly 15 times stronger than the roll. Estimating C_n revealed the strength of the pitch and roll angles in each mode ϕ_n, which was achieved using a modal decomposition method detailed in (*23*).

Experimentally, C remained high across all three web shapes (see Figure 2C), which were fabricated via 3D printing using TPU, a flexible polymer material. Each web was repeatedly impacted at different locations using a micro-hammer instrumented with a force sensor (figure S9). Webs 1-3 showed median values of 5.9, 3.9, and 3.4, with interquartile ranges of 4.6–7.6, 3.5–6.4, and 3.1–4.5, respectively (n=34, 19, and 21). All computational and experimental cases show that C_2 exceeded C_1 by approximately an order of magnitude, demonstrating the strong directional clarity of the second mode, $\phi_{n=2}$. This trend was consistent across the three TPU webs: C_1 exhibited median values of 1.15, 2.5, and 1.45, while C_2 exhibited median values of 11, 15, and 12, with corresponding interquartile ranges depicted in Figure 2C). Unlike the first bell-shaped mode $\phi_{n=1}$, mode 2 $\phi_{n=2}$ was a twisted shape that forced the spider body to experience pitch or roll towards the impact location (Figure 2B).

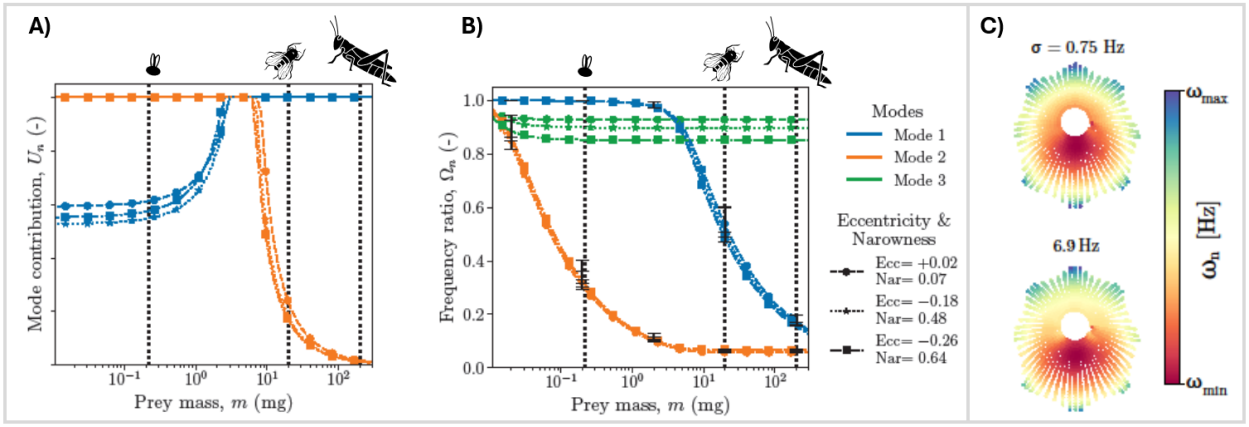

Figure 3: **The web landscape mode shape and resonance shifts reveal a prey's mass.** (**A**) Mode shape contribution U_n is the amplitude at an impact point normalized by the maximum. Contributions of 0 or 1 correspond to no or maximum displacement, respectively, at the impact location. Observe that at least one mode pitches towards the impact location for every possible prey mass. (**B**) Normalized web resonances as a function of a prey mass $\Omega_n(m) = \omega_n(m)/\omega_n^o$. ω_n^o is an empty web resonance. Modes 1 and 2 shift ~90%, compared to only ~16% for higher modes. Modes 1 and 2 exhibit high sensitivity, suggesting that their frequency shifts are effective mechanical decoders of prey mass. (**C**) The maps show the natural frequency ω_n as a function of the prey mass location. The corresponding standard deviations are shown as error bars in **(B)**. Because these are much smaller than the mass-induced frequency shifts, the response is considerably more sensitive to prey mass than to impact location.

The relationship between m_{prey} and amplitude contribution of each mode is given as $(U_n(\mathbf{x}_j) = |\phi(\mathbf{x}_j)|/\max(|\phi|)$, and provided in Figure 3C. The location on the web is x_j. The influence of the prey size on the directional clarity was analyzed by calculating U_n, which described the contribution level of each mode to the pitch towards an impact location (pure pitch: $U_n = 1$, no pitch: $U_n = 0$). The simulations revealed that the low-frequency modes always dominated the webs' collective displacements. The second mode contribution, $U_n = 2$, was dominant for prey masses up to 6.0mg, after which the first mode $U_{n=1}$ dominated. A transition region emerged where both modes pitched toward the prey. Together, these results provided further evidence that the proposed pitch–roll sensing mechanism remained robust across a wide range of prey masses and web geometries, even with substantial variation in web shape and loading.

4 Resonance frequency shifts enable prey mass cue estimate despite signal or environmental noise

Estimating prey mass is likely an early step for spiders to assess prey's potential threat, nutritional value, and escape potential. We hypothesized that the spider used the web's resonant frequencies' sensitivity to the added m_{prey} after impact as a mass cue. This sensitivity was verified computationally for the cases with fixed $m_{prey} = 0.2, 2, 6, 20, 200$mg impacts at all web thread intersection locations, and for a fixed location (marked in 2B) while varying $m_{prey} : 2 \cdot 10^{-4} \rightarrow 2 \cdot 10^{2}$mg by one thousand for all three webs. Figure 3 illustrates the high sensitivity of the normalized resonance ratio, $\Omega_n(m) = \omega_n(m)/\omega_n^o$ to the size of m_{prey}; where ω_n^o is the natural frequency of the empty web for mode n. For m_{prey} between 1.0 and 200mg, Ω_1 decreased by nearly 90% (see Figure 3B). For mode 2, ω_2 exhibited a similar steep decline for a prey mass ranging from 0.01 to 3.0mg. In contrast, the higher modes remained relatively unchanged across the full mass range (maximum drop was 16%). This distinct sensitivity suggests that Ω_1 and Ω_2 enable spiders to estimate prey mass.

While the mass cue was remarkably sufficient, it is important to note that $\Omega_n(m)$ alone did not uniquely provide mass cue clarity if spatial ambiguity arises. The same frequency shift may result from a light prey close to the hub or a heavier prey farther away. This spatial ambiguity was observed in the natural frequencies for $m_{prey} = \{0.2, 2, 20, 20\}$mg at all possible impact locations. See ω_1 and ω_2 maps for a housefly and fruit fly, respectively, Figure 3C. The selected maps corresponded to the highest frequency sensitivity in Web 2, i.e., the steepest slope in Figure 3C. Additional Ω_n and U_n maps are shown in figures S3 and S4.

The spatial ambiguity is quantified by the standard deviation of the natural frequencies σ, as shown in Figures 3A and 3B, and in figures S5 and S6. The maps reveal a systematic pattern: eccentric and narrow webs exhibit greater spatial variability, with σ increasing with geometric asymmetry; e.g., for Web 2, σ increased from 0.64 to 0.88Hz for mode 1 and m_{prey} =20mg, and from 4.4 to 9.4Hz for mode 2 and $m_{prey} = 0.2$mg. Resonance shifts were not determined solely by radial distance from the hub, as in Web 1, but were also shaped by structural asymmetries. Longer web sections, typically at the bottom (*27*), exhibited greater change in the resonance than shorter sections.

In summary. Our findings demonstrate that the orb-weaving spider's instantaneous ability to localize and size prey could be explained by the dynamic interaction between the spider's body and its web. By leveraging the web's high-amplitude and low-frequency, landscape-scale vibrations, the spider may use its entire body as a mechanical gyroscope to extract directional and mass cues—— a mechanism far more robust for impact events than traditional thread-level sensing models. While the first symmetric mode remains stable, the distortion of higher-order modes provides clear directional clarity, and mass-induced resonance shifts significantly outweigh any spatial ambiguity about the impact. Ultimately, this mechanical intelligence of orb webs appears to be key for enabling spiders to thrive for more than 180 million years (*29*) despite the immense natural variation in web geometries and the sensory-rich and noisy environments in which spiders capture prey (*10*). Thus, structures such as webs may provide mechanical intelligence to offload some of the complex neural processing from miniaturized biological systems (*30*).

References and Notes

1. M. Eder, S. Amini, P. Fratzl, Biological composites—complex structures for functional diversity. *Science* **362** (6414), 543–547 (2018).

2. S. Singla, G. Amarpuri, N. Dhopatkar, T. A. Blackledge, A. Dhinojwala, Hygroscopic compounds in spider aggregate glue remove interfacial water to maintain adhesion in humid conditions. *Nature Communications* **9** (1), 1890 (2018).

3. B. Mortimer, A. Soler, L. Wilkins, F. Vollrath, Decoding the locational information in the orb web vibrations of Araneus diadematus and Zygiella x-notata. *Journal of the Royal Society Interface* **16** (2019).

4. S. Kaewunruen, C. Ngamkhanong, S. Xu, Large amplitude vibrations of imperfect spider web structures. *Scientific Reports* **10**, 19161 (2020).

5. N. Morehouse, Spider vision. *Current Biology* **30** (17), R975–R980 (2020).

6. L. E. Robledo-Ospina, *et al.*, Visual antipredator effects of web flexing in an orb web spider, with special reference to web decorations. *The Science of Nature* **110** (3), 23 (2023).

7. J. Zhou, *et al.*, Outsourced hearing in an orb-weaving spider that uses its web as an auditory sensor. *Proceedings of the National Academy of Sciences* **119** (2022).

8. M. B. Talukder, *et al.*, The chemosensory toolkit of the cursorial spider Pisaura mirabilis. *Communications Biology* (2025).

9. X. Nelson, Cognition in spiders: Small brains on eight legs gain traction. *Journal of Zoology* **326** (2), 93–108 (2025).

10. K. Arakawa, *et al.*, 1000 spider silkomes: Linking sequences to silk physical properties. *Science advances* **8** (41), eabo6043 (2022).

11. J. Zhang, *et al.*, Spider-Web-Like Artificial Network for Smart Capture. *Small* **21** (26), 2501687 (2025).

12. V. F. Dal Poggetto, F. Bosia, G. Greco, N. M. Pugno, Prey impact localization enabled by material and structural interaction in spider orb webs. *Advanced Theory and Simulations* **5** (3), 2100282 (2022).

13. J. Wu, T. E. Miller, A. Cicirello, B. Mortimer, Spider dynamics under vertical vibration and its implications for biological vibration sensing. *Journal of The Royal Society Interface* **20** (2023).

14. K. Yavuz, A. M. Soler, R. Zaera, S. Jahangirov, Effect of spider's weight on signal transmittance in vertical orb webs. *Royal Society Open Science* **11** (2024).

15. R. Zaera, Óscar Serrano, J. Fernández-Sáez, A. Morassi, Eco-localization of a prey in a spider orb web. *Journal of Vibration and Control* **28**, 1229–1238 (2022).

16. M. Lott, V. F. D. Poggetto, G. Greco, N. M. Pugno, F. Bosia, Prey localization in spider orb webs using modal vibration analysis. *Scientific Reports* **12**, 19045 (2022).

17. J. E. Niven, S. M. Farris, Miniaturization of nervous systems and neurons. *Current Biology* **22** (9), R323–R329 (2012).

18. H. F. Japyassú, K. N. Laland, Extended spider cognition. *Animal Cognition* **20** (3), 375–395 (2017).

19. L. Marom, M. J. Buehler, Frontiers of biological material intelligence: L. Marom, MJ Buehler. *MRS Bulletin* pp. 1–13 (2025).

20. W. Lu, N. A. Lee, M. J. Buehler, Modeling and design of heterogeneous hierarchical bioinspired spider web structures using deep learning and additive manufacturing. *Proceedings of the National Academy of Sciences* **120** (31), e2305273120 (2023).

21. B. Mortimer, A. Soler, C. Siviour, F. Vollrath, Remote monitoring of vibrational information in spider webs. *The Science of Nature* **105** (5), 37 (2018).

22. M. S. Davies, T. Hesselberg, The use of tuning forks for studying behavioural responses in orb web spiders. *Insects* **13** (4), 370 (2022).

23. Materials and methods are available as supplementary material.

24. T. Masmeijer, P. De, J. Slavič, T. Blackledge, E. Habtour, Code, data, and videos for Gyroscopic Spiders: Web Mechanical Intelligence facilitate prey sensing, Dryad, University of Washington Libraries, doi:10.5061/dryad.pc866t255.

25. Y. Jiang, H. Nayeb-Hashemi, Dynamic response of spider orb webs subject to prey impact. *International Journal of Mechanical Sciences* **186**, 105899 (2020).

26. S. Zschokke, Spiral and web asymmetry in the orb webs of Araneus diadematus (Araneae: Araneidae). *Journal of Arachnology* **39**, 358–362 (2011).

27. M. Coslovsky, S. Zschokke, Asymmetry in Orb-Webs: An Adaptation to Web Building Costs? *Journal of Insect Behavior* **22**, 29–38 (2009).

28. S. Han, H. Astley, D. Maksuta, T. Blackledge, External power amplification drives prey capture in a spider web. *Proceedings of the National Academy of Sciences* **116** (24), 12060–12065 (2019).

29. D. Dimitrov, G. Hormiga, Spider diversification through space and time. *Annual review of entomology* **66** (1), 225–241 (2021).

30. V. Chiara, P. Arrufat, R. Jeanson, A variable refractory period increases collective performance in noisy environments. *Proceedings of the National Academy of Sciences* **119** (12), e2115103119 (2022).

31. K. Zaletelj, *et al.*, ladisk/pyidi: v1.3.3 (2026), doi:10.5281/zenodo.20180382, `https://doi.org/10.5281/zenodo.20180382`.

32. P. Virtanen, *et al.*, SciPy 1.0: fundamental algorithms for scientific computing in Python. *Nature methods* **17** (3), 261–272 (2020).

33. T. Masmeijer, E. Habtour, K. Zaletelj, J. Slavič, Directional DIC method with automatic feature selection. *Mechanical Systems and Signal Processing* **224**, 112080 (2025).

34. A. Soler, R. Zaera, The secondary frame in spider orb webs: The detail that makes the difference. *Scientific Reports* **6** (2016).

35. T. Masmeijer, T. Méndez Echenagucia, J. Slavič, R. Loendersloot, E. Habtour, Effect of eccentricity on sensing in spider web inspired cable nets, in *Journal of Physics: Conference Series* (IOP Publishing), vol. 2647 (2024), p. 192012.

36. T. Masmeijer, C. Swain, J. Hill, E. Habtour, Programming tension in 3D printed networks inspired by spiderwebs. *Materials & Design* p. 115281 (2026).

37. F. Vollrath, M. Downes, S. Krackow, Design Variability in Web Geometry of an Orb-Weaving Spider. *Physiology & Behavior* **62**, 735–743 (1997).

38. E. Wirth, F. Barth, Forces in the spider orb web. *Journal of Comparative Physiology A* **171**, 359–371 (1992).

39. Dassault Systèmes Simulia Corp., Johnston, RI, USA, *Abaqus User's Guide (Version 2024)* (2023), `https://3ds.com`.

40. M. Alam, M. Wahab, C. Jenkins, Mechanics in naturally compliant structures. *Mechanics of Materials* **39**, 145–160 (2007), doi:10.1016/j.mechmat.2006.04.005.

41. S. W. Cranford, A. Tarakanova, N. M. Pugno, M. J. Buehler, Nonlinear material behaviour of spider silk yields robust webs. *Nature* **482**, 72–76 (2012).

42. U. Sahin, I. L. Mathew, D. Singh, Temperature dependent wingbeat frequency response in two weight groups of *Musca domestica*. *International Journal of Entomology Research* **9** (6), 119–121 (2024).

43. D. Porter, J. Guan, F. Vollrath, Spider silk: Super material or thin fibre? *Advanced Materials* **25**, 1275–1279 (2013).

Acknowledgments

The authors express gratitude to Prof. Avin Vijay for providing access to the University of Washington Klone Hyak High Performance Compute Cluster to performed finite element simulation of spider web impact dynamics; Prof. Peter Mackenzie-Helnwein for advice on modeling highly

flexible structures; Min Jung Koo for creating the scientific visualization; and the Illimited Lab members, Victoria Leigh and Keira Morrissey, and John Racy, for their assistant with the experimental efforts. The authors also thank Reagan Rogers and Myah Derderian for their assistance with the mechanical testing of the TPU. Some icons used in this work were sourced from the Noun Project and are used under their free license with attribution. We gratefully acknowledge the creators: Marie van den Broeck, Panji, and Lars Meiertoberens.

Funding: The authors acknowledge the support of the US National Science Foundation CAREER Award (Grant No. 2440838), and the Slovenian Research Agency (Research Core Funding No. P2-0263).

Author contributions: Conceptualization: T.C.P.M., J.S., T.A.B, E.H. Methodology: T.C.P.M., J.S., T.A.B, E.H. Software: T.C.P.M., J.S., E.H. Validation: T.C.P.M., E.H. Formal Analysis: T.C.P.M., E.H. Investigation: T.C.P.M., J.S., T.A.B, E.H. Resources: T.C.P.M., J.S., T.A.B, E.H. Data curation: T.C.P.M., Writing – original draft: T.C.P.M., E.H. Writing – review & editing: T.C.P.M., J.S., T.A.B, E.H. Visualization: T.C.P.M., E.H. Supervision: E.H. Project administration: E.H. Funding acquisition: J.S., E.H.

Competing interests: The authors declare no competing interests.

Data and materials availability: The datasets generated and analyzed during this study are available from the corresponding author on reasonable request. The GitHub repository includes Python code for image and signal processing, system identification, and plots using pyIDI (*31*) and Scipy (*32*).

Animal role in the study: Mature female a. trifasciata were housed in standard laboratory conditions. They were used solely for high-speed video recording of their locomotion in response to prey impacts on the web.

Animal experimental procedures: No human-related datasets were used in this study. No experimental modifications or invasive testing were performed on the live spiders. The methods used were non-contact and did not compromise the spider's welfare. Following the video collection procedures, the spiders were safely released back into their natural habitat.

Supplementary materials

Materials and Methods; Figs. S1 to S12; Table S1; MDAR Reproducibility Checklist; and Movies S1 to S2.

Supplementary Materials for

Spiders' Gyroscopic Motion via Web Mechanical Intelligence Facilitates Prey Sensing

First Author[*†], T.C.P. Masmeijer[†], J. Slavič[†], P. DE [†], T.A. Blackledge[†], E. Habtour[1*†]

[*]Corresponding author. Email: habtour@uw.edu

This PDF file includes:

Materials and Methods

Figs. S1 to S12

Table S1

References

Other Supplementary Materials for this manuscript:

MDAR Reproducibility Checklist

Movies SV1.mp4 to SV2.mp4

Simulation code and data: Finite_Element_Abaqus_Files.zip

Materials and Methods

Image tracking of spider pitch-roll motion on the web due to a cricket impact

High-speed, high-resolution Digital Image Correlation (DIC) was used to capture and analyze a spider's body motion in response to vibrations in its web when prey impacts the web. For this study, 10 high-speed videos were collected of mature female *Argiope trifasciata* (*Araneae*: *Araneidae*, ~150mg) spiders residing at the hub of their web, intercepting freely jumping crickets (*Gryllodes sigillatus*, ~100mg). The impact events were recorded at 125 frames per second at 12-bit resolution using a high-speed video camera (maker: Photron, model: SA4). The camera was positioned perpendicular to the plane of the web. To ensure proper contrast for tracking the spider's pitch and roll motion and adequate high-resolution to capture the vibrations of each thread, the web landscape and its surrounding environment were illuminated with a high-power LED panel (maker: Fovitec, model: S-900D), positioned laterally to the web. Specific points on the spider's abdomen were automatically selected to track the spider's pitch and roll angles using the Shi-Tomasi detection algorithm (*33*). Examples of those points are shown in Fig. S1. The displacements of keypoints were tracked using the DIC technique with a 9×9 pixel window (*33*). The DIC code for tracking the points is available in (*31*). The spider's pitch and roll angle calculations are detailed in the experimental section below. Images of spiders' rotational motion due to prey impact from the 10 video-recorded experiments are shown in Fig. S2. All ten experiments showed that a spider's body rotated toward the direction of prey impact, within a maximum detection time of 35 ± 2 ms.

Simulating web dynamics due to variation in its geometries, prey masses, and prey locations

This study simulated three distinct web geometries with increasing narrowness (Nar) and eccentricity (Ecc), shown in Fig. 2A. All webs shared the same structural links, which consisted of 56 radial threads, 19 spiral turns, and the inclusion of a secondary frame known to maintain mechanical integrity (*34*). The full web geometries were generated using the Force Density Method (*35, 36*) to satisfy static equilibrium and to follow tension gradients and structural layouts reported in biological studies (*37, 38*). The force density method linearizes the static force equilibrium equations, enabling the fast form-finding of the web's network with desired Nar and Ecc shape parameters

using tension gradients. The force density of each link i in the web is determined using:

$$q_i = \frac{F_i}{l_i}, \qquad F_i = EA\frac{\Delta l_i}{l_i} \tag{S1}$$

where link i tension force and length are F_i and l_i, respectively. The link material Young's modulus and cross-sectional area are E and A, respectively. Python code was developed to generate webs with desired shapes using force-density methods. The code also imports the geometries to Abaqus 2024, a commercial Finite Element Method (FEM) package (*39*). The Python code and FEM input files are available in (*24*).

To systematically isolate the effects of prey mass on vibrational response, FEM models of the three web shapes (Web 1, 2, and 3) were developed to investigate the robustness of the pitch-roll sensing mechanism. Each link of the web was discretized into 15 3-dimensional truss elements (using Abaqus T3D2 2-node linear displacement truss element). Each node has three translational degrees of freedom with only axial force support. This ensured that the web links behaved as tension-only members only, i.e., like strings. A subdivision of 15 elements per link was chosen to sufficiently capture the smooth spatial gradients of the vibration mode shapes, as verified by a convergence analysis.

The orb-web geometries and silk densities found in nature and used in this study are specified in Table S1 (*37, 40*). While spider silk exhibits geometric and material nonlinearities, this study linearized the material response using pre-stress values typically observed in radial, spiral, and mooring threads (*41*), which shows the local material deformation was well within the elastic regime, as shown by the authors in a different study of prestressed polymer materials (*36*). While constitutive nonlinearities are expected to influence the quantitative response at larger impact amplitudes, they were not expected to alter the qualitative mechanism of the early directional pitching motion identified here. The linearized Young's modulus values used were: $E_{\text{mooring}} = E_{\text{radial}} = 10\text{GPa}$, and $E_{\text{spiral}} = 0.14\text{MPa}$. Fixed boundary conditions were applied at all outer attachment points. The spider was modeled as a concentrated point mass of 20 mg at the central node. The prey was modeled similarly, with its mass and location varied across simulations. The prey masses considered across all intersections between radial threads and the catching spiral were 0.2, 2.0, 6.0, 20, 200 mg. Spatial mapping of each web required 5320 simulations of five different masses impacting 1064 intersections (56 radials × 19 spiral turns). This totaled 15900 for three web designs. The (*Araneus*

diadematus) mass is 20 mg (*3*). The mass of a fruit fly (*Drosophila melanogaster*) is approximately 0.219-0.304mg (*42*), and the mass of a typical house fly (*Musca domestica*) is 20 mg (*42*). For the mass mapping, 1,000 different prey mass levels were investigated for each web, resulting in an additional 3,000 simulations. The prey mass at the locations marked in Fig. 3C to generate Figs. S1 to S8. The prey masses were distributed logarithmically between 2×10^{-4}mg and 2×10^{2}mg. The dynamic analyses yielded the eigenvalues ω_n (natural frequencies) and the eigenmodes ϕ_n, which were normalized to their respective mode maxima. Subsequently, the normalized natural frequencies and deflection mode shapes as a function of prey masses and location are reported in Figs. S1 to S8.

Experimental study of artificial web dynamics due to variation in its geometries, prey locations

The experimental investigation focused on how changes in web shape and prey location affected the robustness of the pitch-roll sensing mechanism. The prey mass was not varied since the objective was to validate the computational models. Three different spider web shapes were designed; namely, Web 1: centric with no narrowness (Ecc=0.03 and Nar=0.07); Web 2: moderately eccentric and narrow (Ecc=-0.18 and Nar=0.48); and Web 3: highly eccentric and narrow (Ecc=-0.26 and Nar=0.64). The three shapes shown in Fig. 2A were 3D printed using a high-precision additive/subtractive manufacturing system (Maker nScrypt, model 3nD). The webs were made of Thermoplastic Polyurethane (TPU) with a Young's modulus $E = 200$ MPa (*36*), owing to its high flexibility. Each web was printed as a single layer with a cross-sectional area of 0.2×0.4mm^2. Artificial masses were added to the fabricated web structures to simulate the inertia of the spider and prey, as shown in Figs. S9 and S10. The spider, prey, and web masses were 48g, 0.60g, and 1.2g, respectively. Each web structure was suspended from its eight anchors to a rigid hexagonal frame. Each anchor was secured to the frame through an interface that consisted of a tension screw and a micro force tension sensor (Vendor: RobotShop, Model: CZL635), as shown in Fig. S9. The interfaces ensured that the web threads (links) maintained the intended tension gradient derived from the FEM models. The tension at the anchors was monitored using a National Instruments data acquisition system (Model: NI9237).

The prey-impact excitation was simulated in the out-of-plane direction using a micro-hammer with a force sensor. Illumination was provided by two 50 kLumen LED lights, one above and

one below the web, with a light-diffusing panel beneath to create high contrast between the black web and the white background. Displacements of the web and spider were retrieved using motion extraction methods (Figs. S10 and S11). Nineteen prey impact locations were selected for each web (Fig S12. A Photron Fastcam SA-Z equipped with a Sigma 180mm F2.8 Macro lens captured the response of the spider web-like structures at 8,000 frames per second, recording 8,000 grayscale images of 1,024 × 512 pixels at 12-bit resolution. The displacements of keypoints of the web-like structures were retrieved using a combination of DIC and Directional-DIC (*33*).

Points on the web were selected at local maxima in a score image defined by the absolute vertical gradient within a 3-by-3 window, which also served as the tracking window in D-DIC. For DIC, corner keypoints were extracted using the Shi–Tomasi corner detection algorithm (*33*) with 7-by-7-pixel windows. The distribution of DIC and D-DIC keypoints used in Fig. 2 is shown in Fig. S11.

Extracting the spider pitch-roll motion, and web's deflection mode shapes, and natural frequencies due to impact from videos

For the natural and artificial webs, extracting the vibration deflection mode shapes, ϕ_n, and their associated resonance (natural) frequencies, ω_n, was accomplished by calculating the Frequency Response Functions (FRFs) from the measured displacements and the impact force signals, as shown in Fig. S12. Next, the modal decompositions were computed using the PolyMAX method (*43*). The pitch-roll angles θ were calculated for the region near the spider, which was divided into two symmetric sections separated by a neutral axis, as shown in Figs. 1C and S11 for the real and artificial spiders, respectively. The prey direction defined the unit vector $\mathbf{n}_{\text{roll}}$, which served as the neutral axis for calculating roll. The neutral axis for calculating pitch was defined by the unit vector $\mathbf{n}_{\text{pitch}}$, which was orthogonal to $\mathbf{n}_{\text{roll}}$.

The dynamics of the points on the web were tracked from the videos using the DIC method. For the video of a cricket impacting the web, the key points were on or near the spider's abdomen (see Fig. 1C and Movie S1). The displacement points of the artificial spider webs were defined at the intersections near the hub (see Fig. S12 and Movie S2). For each tracked point i, $\mathbf{x}_i$ was assigned to be its position relative to the spider's center, and u_i was its measured out-of-plane displacement. To this end, the signed distance r_i to the neutral axis can be expressed as the dot product $r_i = \mathbf{x}_i \cdot \mathbf{n}$,

where $\mathbf{n}$ is either $\mathbf{n}_{\text{roll}}$ or $\mathbf{n}_{\text{pitch}}$, depending on which inclination was being computed. The sign of r_i indicates which side of the neutral axis the point lies on. The inclination can be calculated as the average normalized displacement across N nodes:

$$\theta = \frac{1}{N} \sum_{i=1}^{N} \frac{u_i}{r_i} \tag{S2}$$

with θ_{pitch} and θ_{roll} computed using the respective neutral axes. This formulation captured the angular response of the web structure near the spider and provided a physically meaningful cue for directionality. To determine the mode-specific cue C_n, the inclination was determined for the mode shape ϕ_n as opposed to the displacement u.

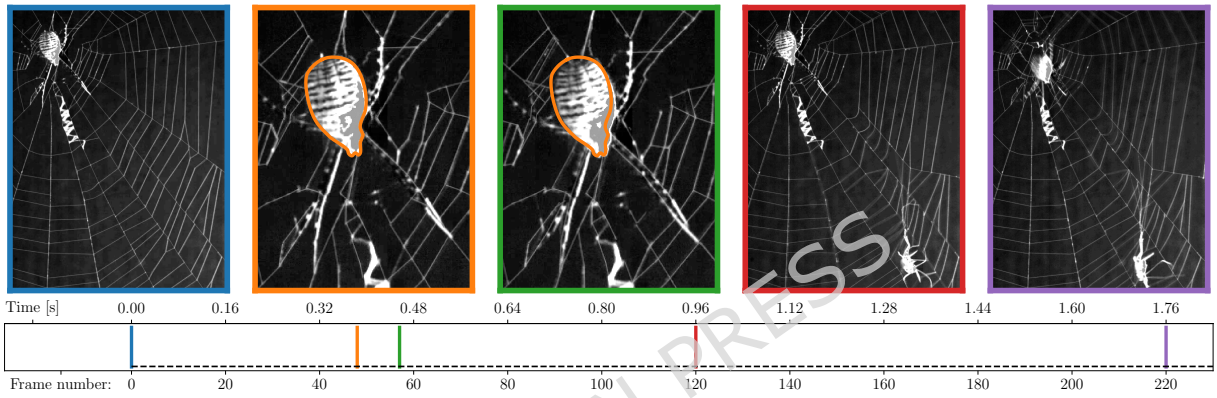

Figure S1: **Image sequences of *Argiope trifasciata* spider using pitch-roll to reorient toward cricket impacting its web.** From left to right; Spider and web at rest (blue), the spider immediately before the cricket impacts the web (orange) (the spiders' abdomen is annotated), the spider pitches towards the impact location (green) (with same annotation as on previous frame), the web with the cricket at its final position in the web (red), and the spider's first observed response to the impact (purple). The frames in this figure are post-processed in Adobe Photoshop solely to improve the images' contrast. Full video available in Movie S1.

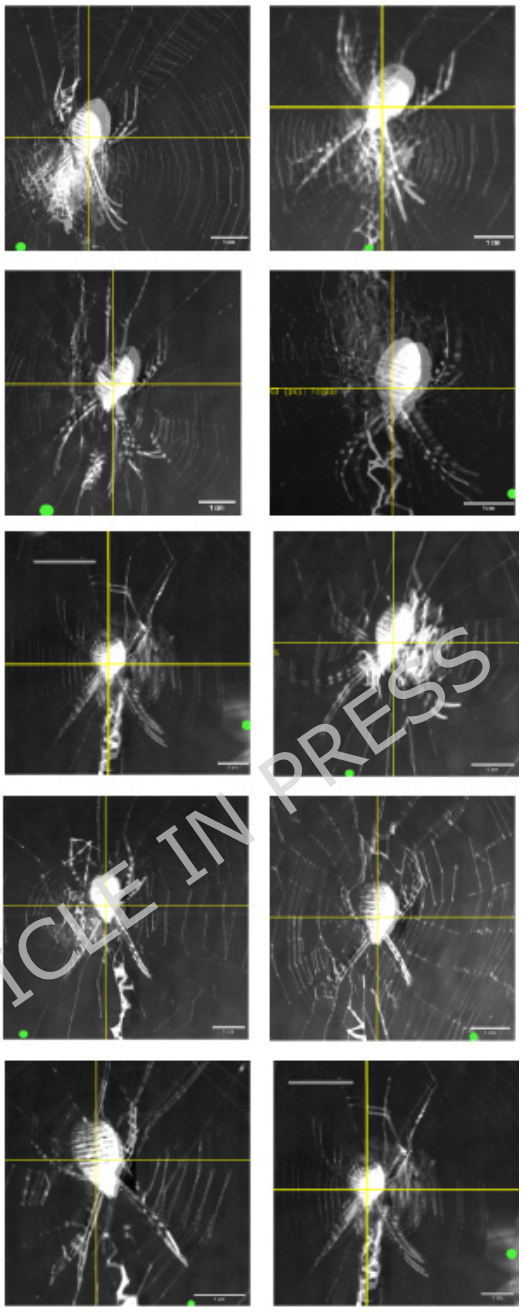

Figure S2: **Images of rotational motion of spiders during prey impact (crickets jumping into the webs).** The images were obtained from high-speed videos of ten impact experiments. All images show the spider body rotating toward the direction of prey impact, reaching a maximum within 35 ± 2 ms. In each image, the spider's position before impact is the solid image and its position during the maximum observed rotation is the translucent overlay. The green dot on each image shows the direction of the prey impact. An example full video is available in Movie S1.

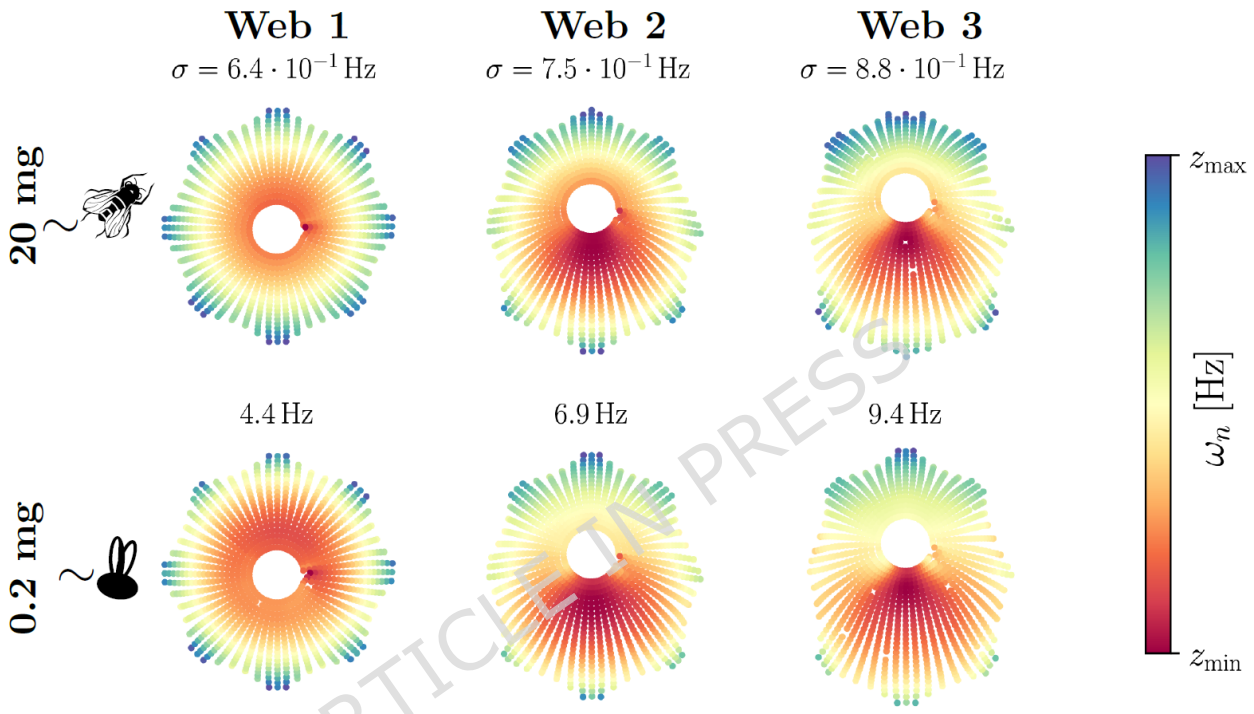

Figure S3: **Mapping the change in the web natural frequency with prey mass and impact location.** Columns are the normalized natural frequency maps for mode 1, showing how the natural frequency varies with impact mass and location. The location of the lowest and highest natural frequency shifts for the given prey mass are the $z_{\min}$ and $z_{\max}$, respectively. The standard deviation, σ, in the natural frequencies due to location is provided for each map.

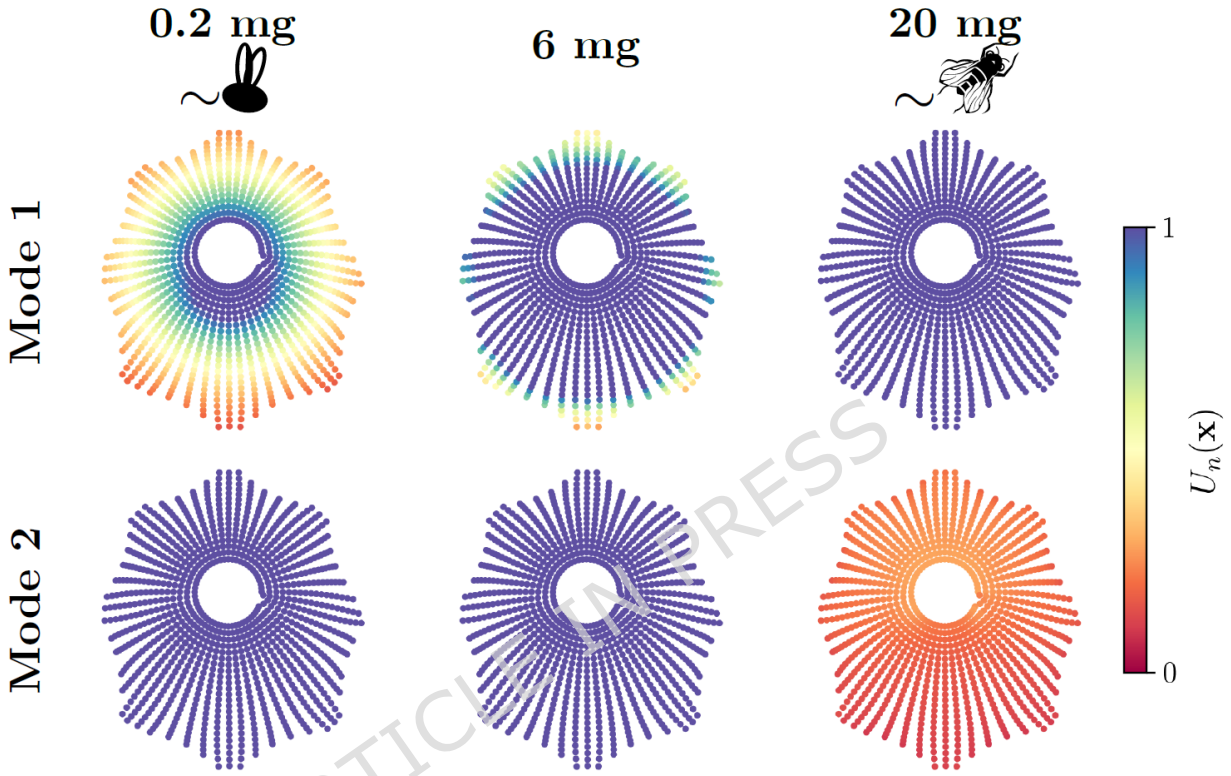

Figure S4: **Examples of normalized maps of Web 2 deflection or shape contribution, U_n, as a function of different prey masses and impact locations on the web**. For brevity, the figure shows only modes $n = \{1, 2\}$ and $m_{prey} = \{0.2, 6, 20\}$mg. In general, the spider pitches toward the impact location when the relative mode shape contribution is $U_n = 1$. For $m_{prey} = 6$mg, mode $n = 1$ dominates the pitching motion to the impact location over mode $n = 2$, and at least one of the modes conveys prey direction at all tested masses and locations. Mode maps of all webs can be found in Figs. S7 and S8.

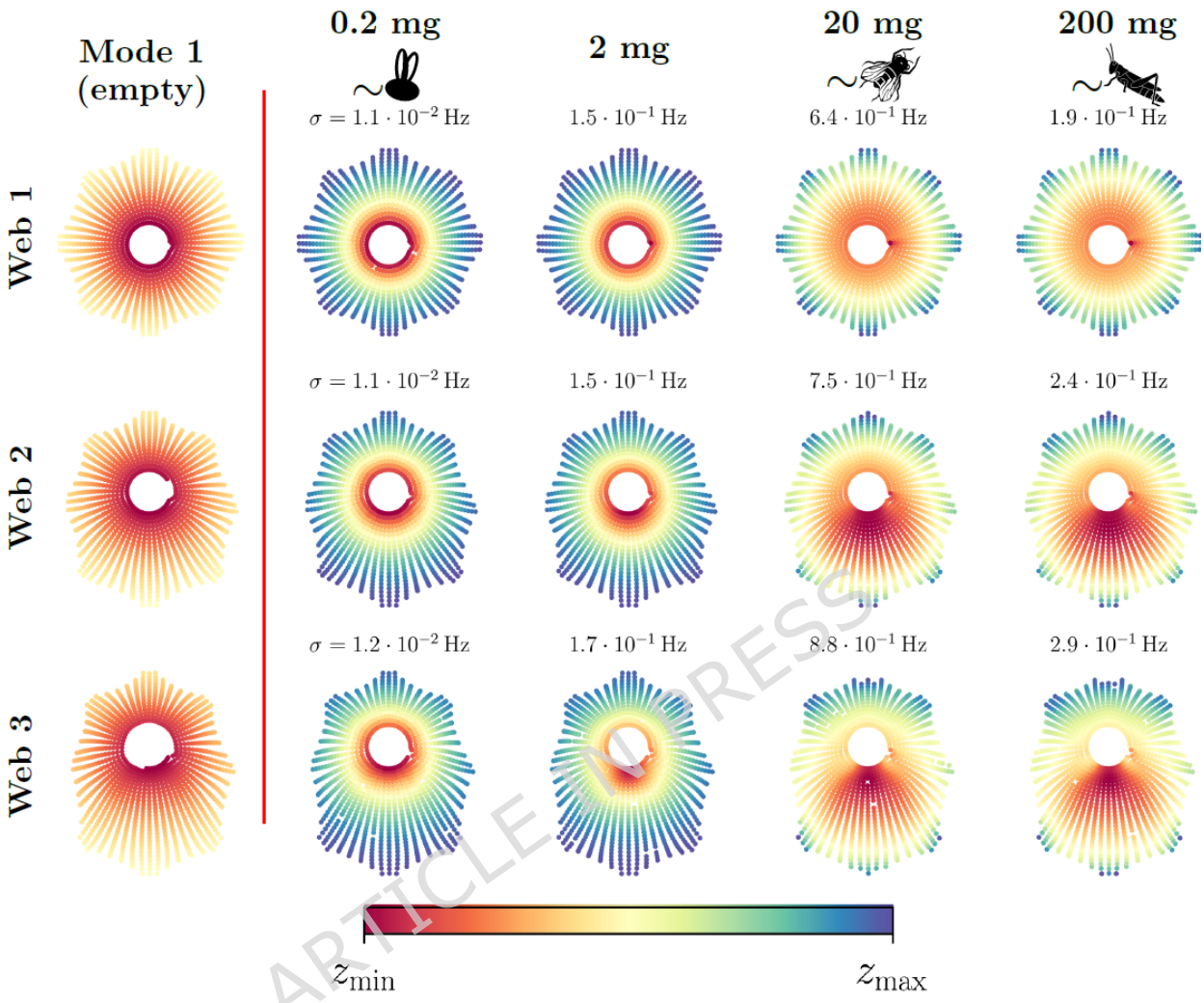

Figure S5: **Mapping the natural frequency Ω_n shifts due to impact location depicted as points on each map for mode $n = 1$.** Each map represents a fixed web shape (Web 1, 2, or 3) that is either empty or impacted by a specified prey mass. The first column shows the empty deflection shapes for mode $n = 1$. The remaining columns are the natural frequency maps, normalized so that Ω_n ranges from $z_{min} = -1$ to $z_{max} = 1$. The changes in $\Omega_{n=1}$ within each map indicate a shift in natural frequency due to the impact location. In contrast, the changes between maps within a column represent the effect of the web shape, which appears to be minimal at low prey masses but significant at high masses. The standard deviation, σ, of the natural frequencies is reported for each map.

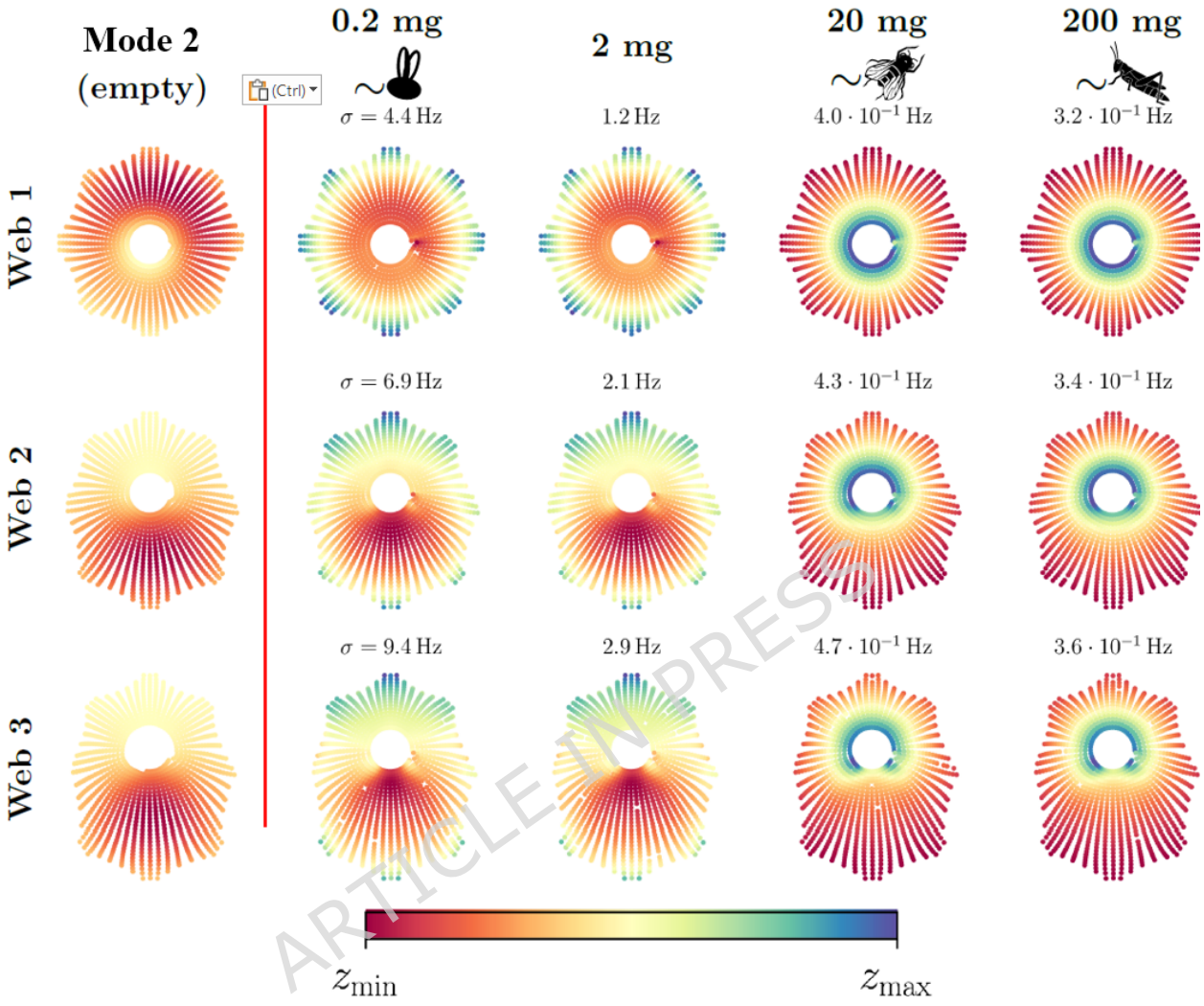

Figure S6: **Mapping the natural frequency Ω_n shifts due to impact location depicted as points on each map for mode $n = 2$.** Each map represents a fixed web shape (Web 1, 2, or 3) that is either empty or impacted by a specified prey mass. The first column shows the empty deflection shapes for mode $n = 2$. The remaining columns are the natural frequency maps, normalized so that Ω_n ranges from $z_{min} = -1$ to $z_{max} = 1$. The changes in $\Omega_{n=2}$ within each map indicate a shift in natural frequency due to the impact location. In contrast, the changes between maps within a column reflect the effect of the web shape, which appears minimal at low prey masses but significant at high masses. The standard deviation, σ, of the natural frequencies is reported for each map.

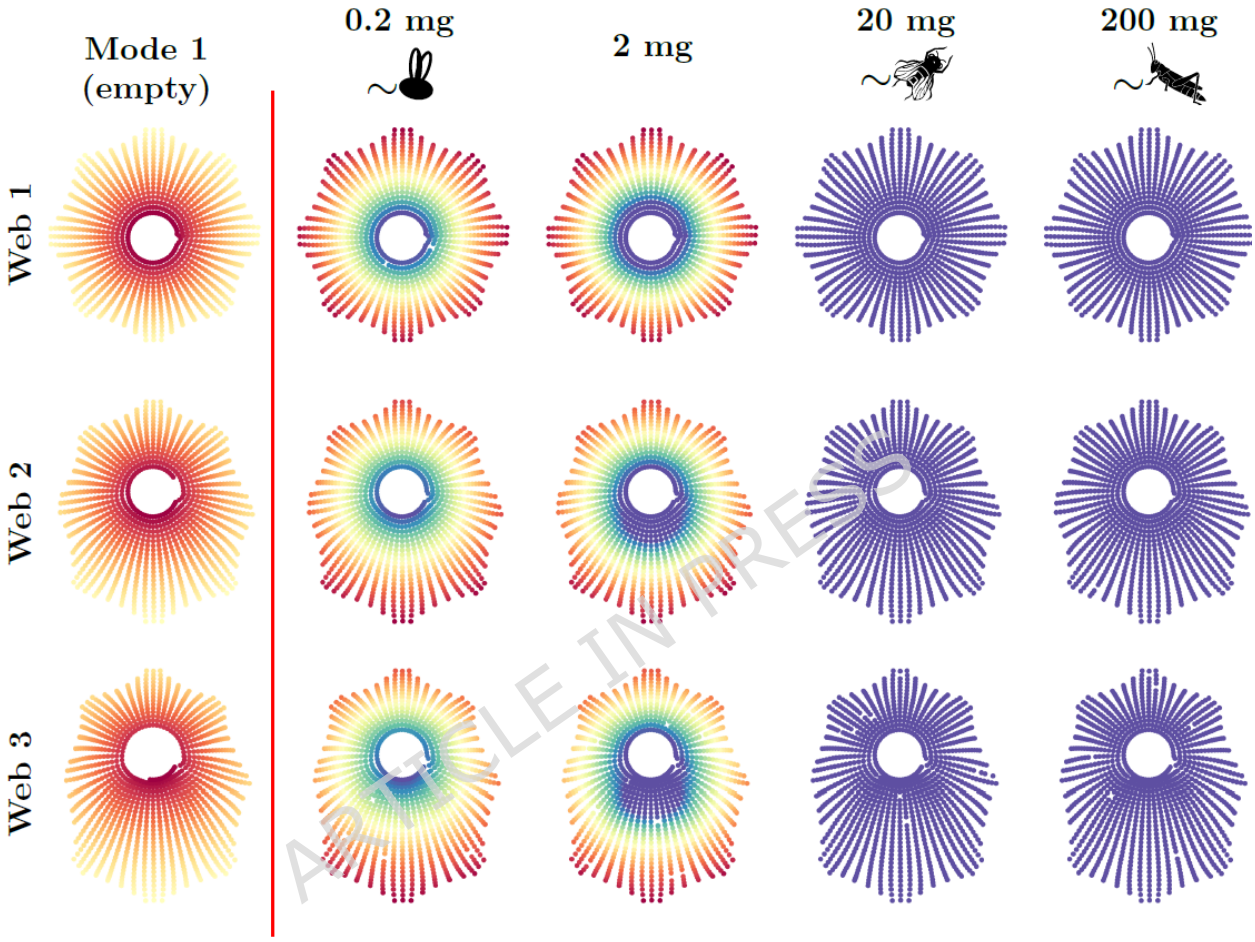

Figure S7: **Mapping the change in the vibration deflection amplitude, U_n, due to impact location depicted as points on each map for mode $n = 1$.** Each map represents a fixed web shape (Web 1, 2, or 3) that is either empty or impacted by a specified prey mass. The first column shows the empty deflection shapes for mode $n = 1$. The remaining columns show the contribution of the deflection amplitude, normalized such that $z_{min} = 0$ and $z_{max} = 1$.

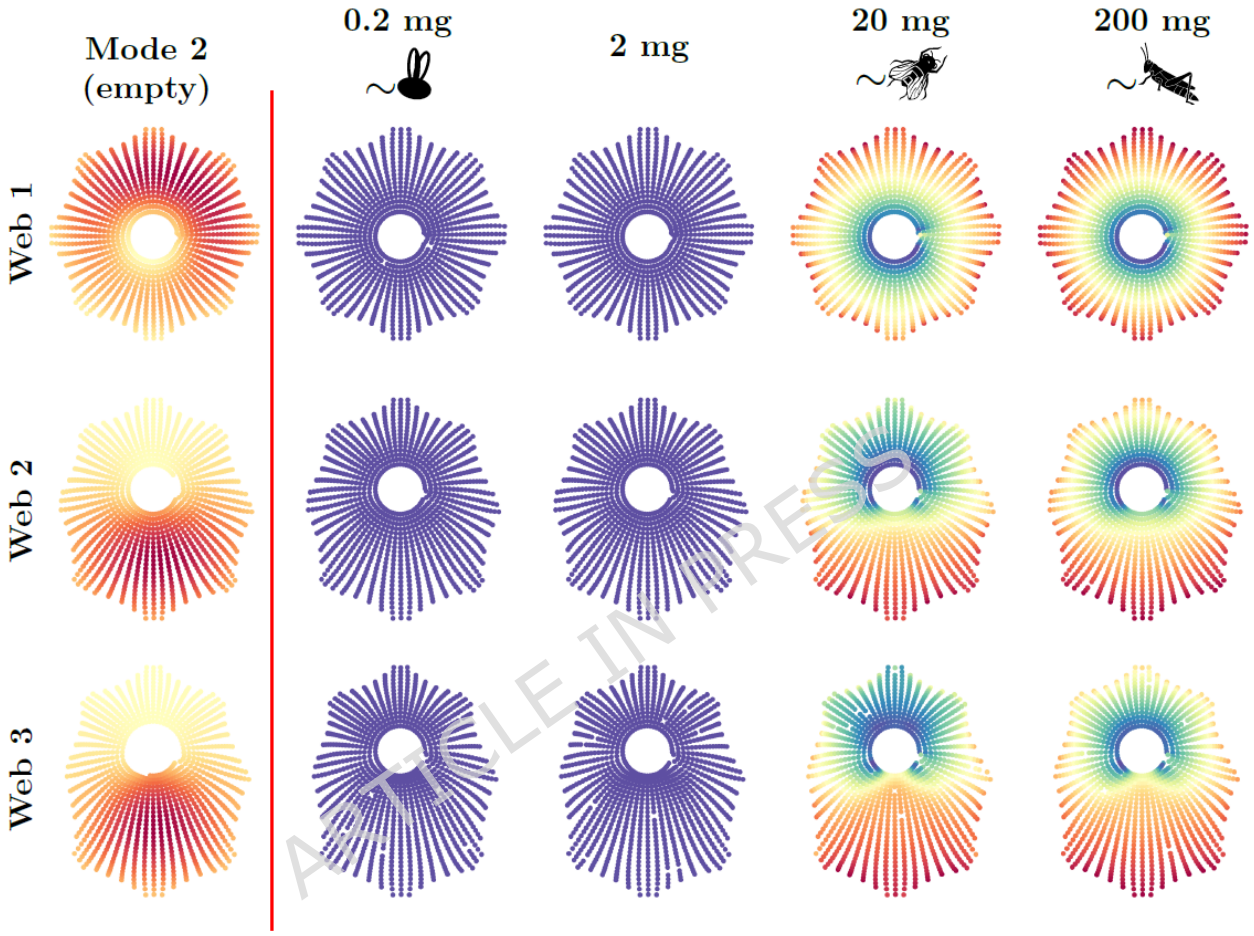

Figure S8: **Mapping the change in the vibration deflection amplitude, U_n, due to impact location depicted as points on each map for mode $n = 2$.** Each map represents a fixed web shape (Web 1, 2, or 3) that is either empty or impacted by a specified prey mass. The first column shows the empty deflection shapes for mode $n = 2$. The remaining columns are the contribution of the deflection amplitude, normalized such that $z_{min} = 0$ to $z_{max} = 1$.

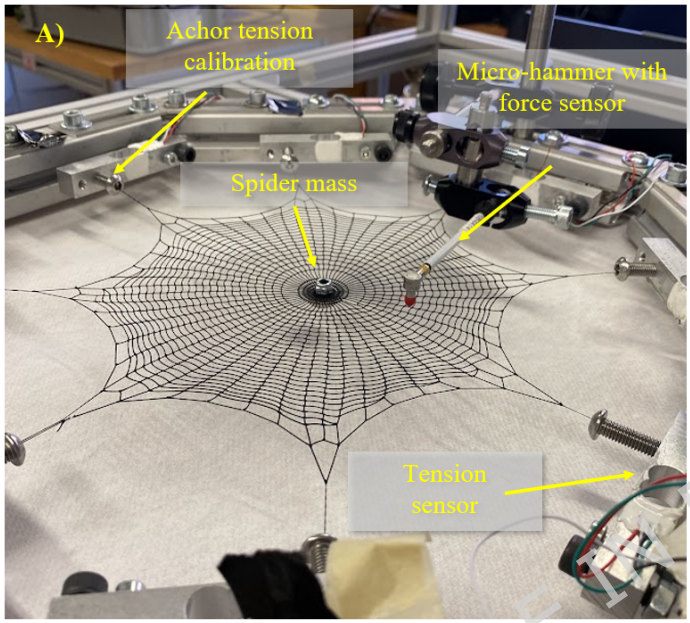

B) Tension sensor at each anchor

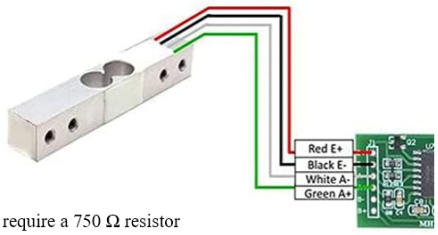

EX+ and EX- require a 750 Ω resistor

Red	E+	Al+ / SC
Black	E-	AL-
White	A-	RS+ / EX+
Green	A+	SC / EX-

$$F = EA\frac{\Delta L}{L_o}$$

Figure S9: **Experimental setup for investigating the dynamics of the artificial webs (Web 1, 2, or 3) due to impact simulated by a micro-hammer.** (**A**) Each web is anchored in the hexagonal frame at eight locations equipped with tension knobs and sensors. The impact is simulated using a micro-hammer, and a force sensor records the impact signal. The hammer strikes the prey mass, which is not shown in this figure. An example of prey mass located on an artificial web is shown in Fig. S10. The Spider mass is simulated with a dead mass at the hub. (**B**) An aluminum tension sensor is used to calibrate the anchor tensions by measuring the strain, $\Delta L/L_o$. Knowing the Young's modulus, E, and cross-sectional area, A, the axial force F can be calculated.

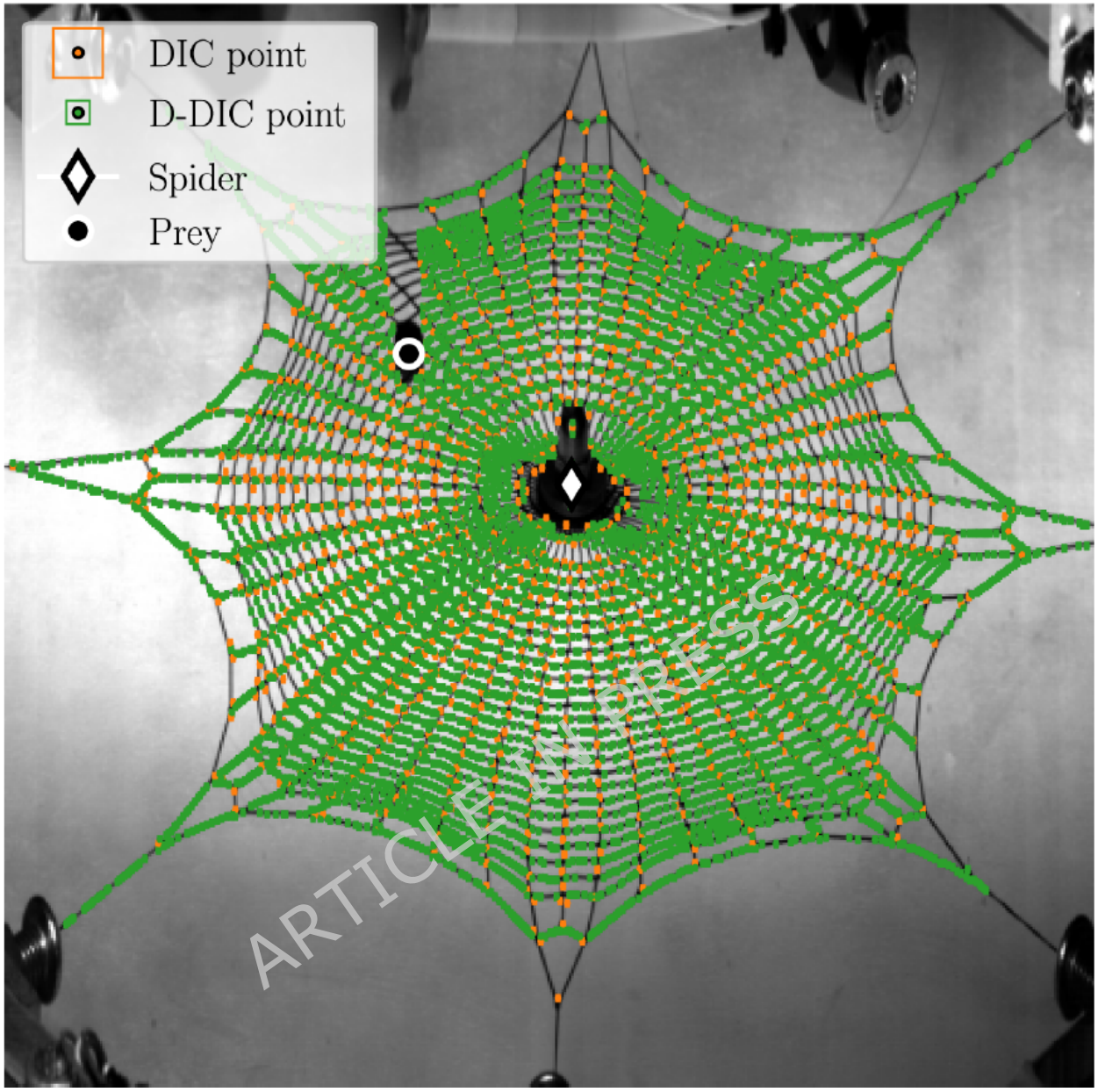

Figure S10: **Direct Digital Image Correlation (D-DIC) method is used to capture the dynamics of the spider, prey, and web**. The D-DIC method automatically selects corner-like (orange) and edge-like (green) points on the web and tracks their motion, as well as edge-like keypoints on the spider web. The lab-simulated spider and prey masses are shown with diamond and circle markers, respectively. The impact is simulated using a micro-hammer that strikes the prey mass indicated by the circular marker. The web displacement response of each point (orange or green) is used to perform the experimental modal analysis to generate the vibration mode shapes in Figs. 2 and S12. The code for extracting the FRF is available in (*31*). An example D-DIC time history dataset is included in the data repository (*24*)

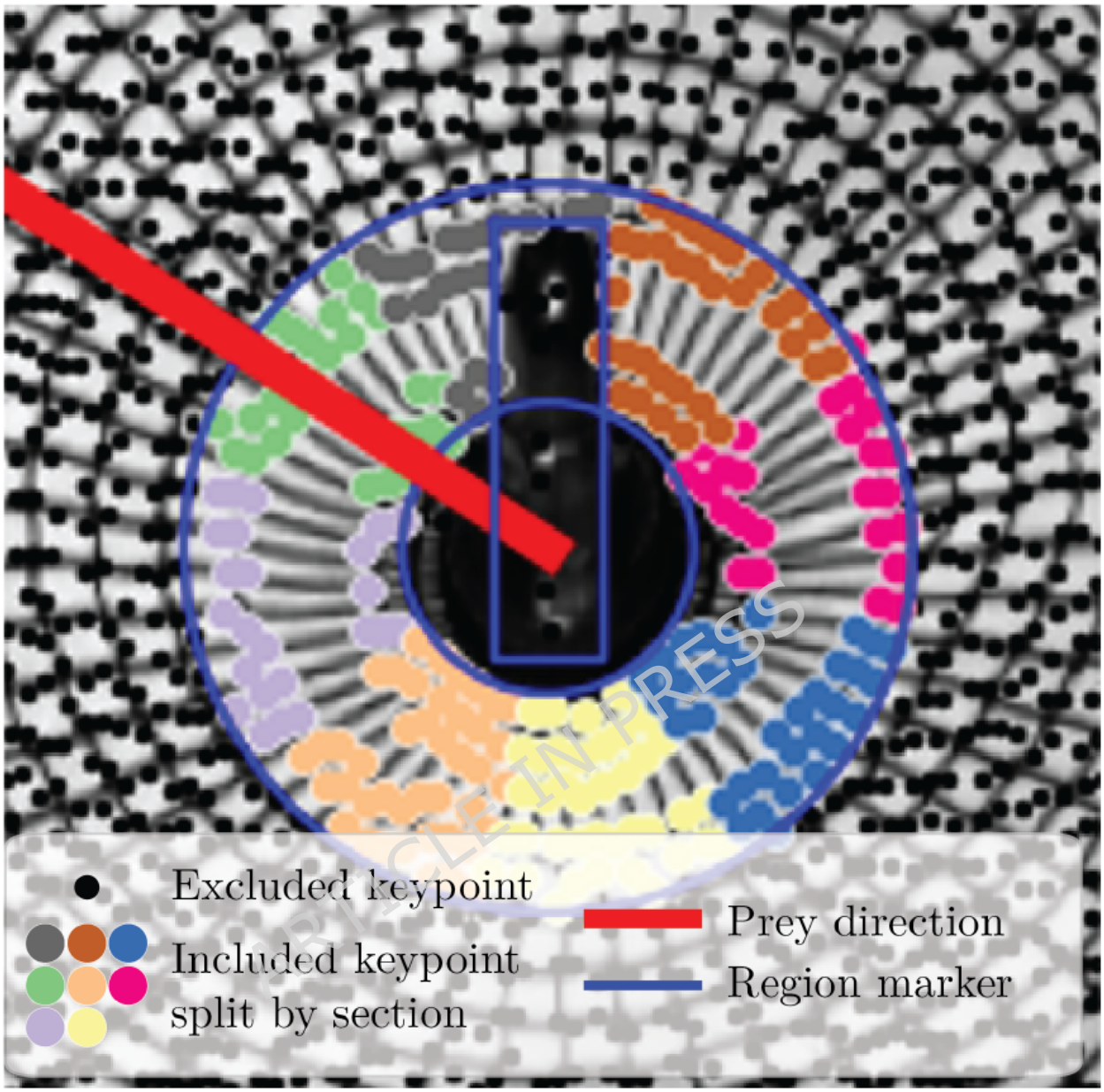

Figure S11: **Digital Image Correlation (D-DIC) of the points of the web's hub is used to estimate pitch and roll angles.** To quantify the directional clarity cue, C, only the corner-like features at the hub are collected. The included points are outside the spider mass (black mass) with inner and outer diameters of 40 and 100 pixels, respectively; see the two purple circles in the middle. Points are excluded if they lie within the rectangle that overlaps the mass. The rectangle has dimensions 15×60 pixels. The included points are split into 8 sections to determine C, as described in (*23*). This sample image corresponds to Web 1 and impact location 1. However, the same procedures are performed on all webs and impact locations.

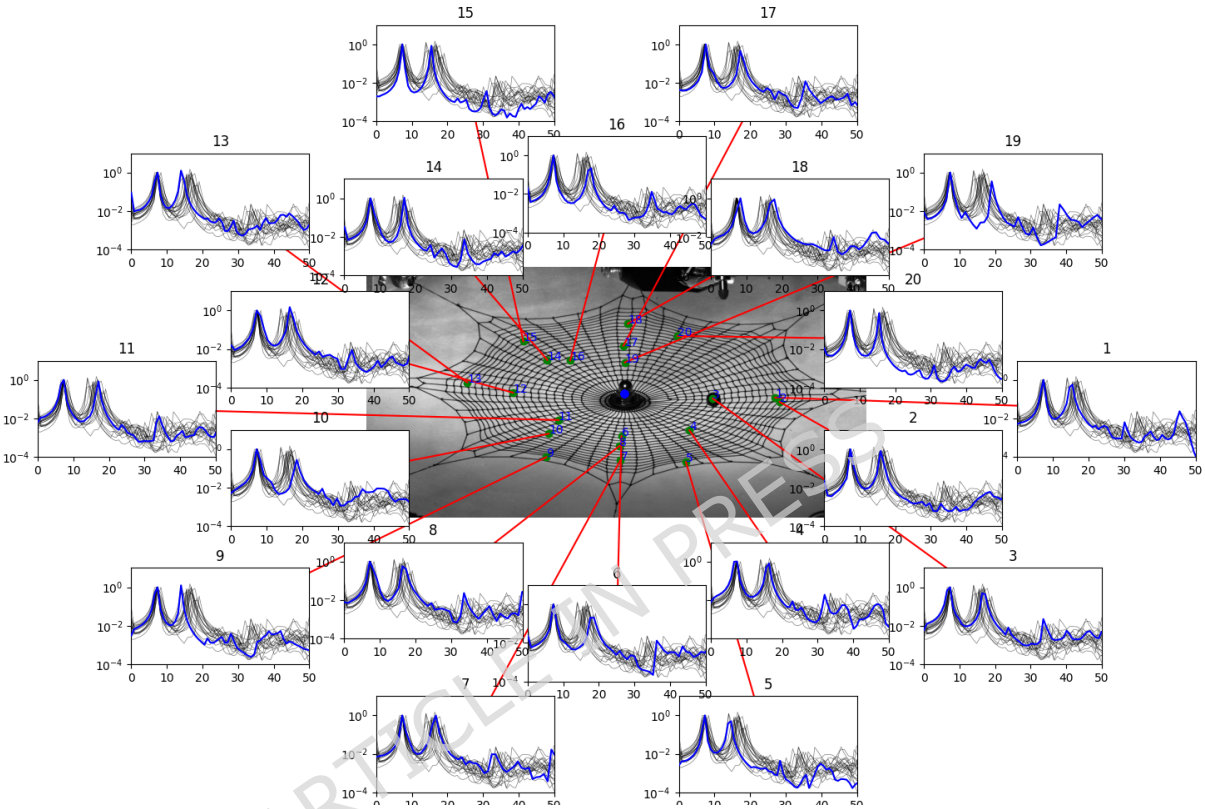

Figure S12: **Illustration of calculated frequency response functions (FRFs) calculations at several locations on an artificial web.** Each Inset figure is an FRF, which is the web response at the specified location determined by the input force at each frequency. Each FRF in blue is the average of several experiments shown as gray curves. From the FRFs, the resonance frequency shifts are tracked as functions of prey mass and location. While in our studies, we tracked hundreds of location points (Fig. S10), we show only a few for graphical clarity. The code for extracting the FRF is available in (*31*).

Table S1: **The *Argiope trifasciata* spider's web geometric and mass properties**. The orb web properties of the spider are obtained from (*37, 40*) to estimate the total mass of a spider web, which is 0.0141 mg.

Property	**Frame/Anchoring**	**Radials**	**Spirals**
Diameter (μm)	5	3.5	2.3
Length (mm)	40.0(Anchoring) + 22.3(secondary frame)	33 radials × 30	500
Density	ρ = 1098 kg/m^3		

Movie S1. Tracking the pitch-roll motion of an actual spider utilizing its body when a cricket impacted its web. The unfortunate (*Gryllodes sigillatus*) cricket can be observed in this video hitting an orb web (*Argiope trifasciata*). The spider rapidly senses the direction of the impact. The video is analyzed using the digital image correlation method detailed in (*23*). The main results are summarized in Fig. 1. The computed directional cue strength indicates that the pitch is 14.8 times greater than the roll, suggesting the spider clearly pitches toward the prey. Movie S1 is publicly available for download from (*24*).

Movie S2. Dynamics of an artificial web with a spider-like mass due to a prey mass simulated with a micro-hammer. A high-speed, high-resolution camera is used to capture the motion of the web and the representative spider and prey masses. Digital image correlation (DIC) time-history data for points on the web (Fig. S10) are used to calculate the frequency response functions (Fig. S12). A summary of the results is provided in Fig. 2. Movie S2 is publicly available for download from (*24*).